ACS Sustainable Chemistry & Engineering

pubs.acs.org/journal/ascecg

Research Article

UV-Sensing Cellulose Fibers Manufactured by Direct Incorporation of Photochromic Minerals

Wenwen Fang,* Emma Sairanen, Sami Vuori, Marja Rissanen, Isabella Norrbo, Mika Lastusaari, and Herbert Sixta*

Cite This: *ACS Sustainable Chem. Eng.* 2021, 9, 16338−16346

Read Online

ACCESS | Metrics & More | Article Recommendations | Supporting Information

ABSTRACT: Textile-based wearable sensors integrated into daily wear offer opportunities for on-demand, real-time self-diagnosis to monitor health conditions with changing environmental surroundings and hazards. One still underrated environmental hazard is accumulated UV irradiation, causing skin burns, accelerated aging, and skin cancers. Here, we have demonstrated a sustainable fiber manufacture process to integrate photochromic hackmanite micro-particles directly into a cellulose body to achieve UV-sensing functionality in daily-life textiles. The hackmanite particles were dispersed into an ionic liquid cellulose dope using ultrasonication and nanofibrillated cellulose as a dispersant, resulting in good spinnability. The obtained fibers possess high mechanical strength with up to 10% photochromic hackmanite loading. To demonstrate its application in wearable UV sensors, the fibers were spun into yarn and then knitted into a piece of jersey fabric. The coloration of hackmanite-incorporated textiles under UV irradiation is readily quantified by image analysis using red−green−blue ratios, which was further utilized for UV dosimetry with a smartphone application showcasing the practical use of the UV sensor. The UV-sensing functionality remained the same after intensive washing and abrasion tests, further demonstrating the feasibility of its application in everyday garments.

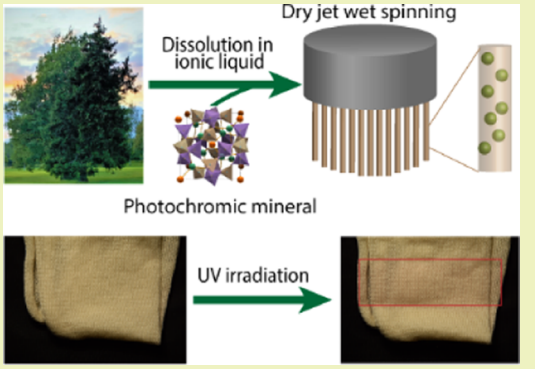

KEYWORDS: *dry jet wet spinning, regenerated cellulose, smart textiles, hackmanite, ionic liquid*

INTRODUCTION

In the course of individualized medical applications, wearable technology and mobile healthcare are playing a key role in monitoring people's conditions in real time, thus proactively improving the quality of life.[1,2] Among an enormous number of conceptualized wearable sensors, the majority of them are thin-polymer-film-based and worn with skin contact, which could cause skin irritation over time and reduced the acceptance of wearable sensors.[3] Combining the advantages of lightweight, flexibility, and comfort on touch, textile-based sensing systems offer a potential platform for the human body to incorporate sensing and control.[1,4] In order to make textile-based wearable sensors available for market-ready innovations, efficient and sustainable textile-manufacturing techniques that integrate new functionalities into existing garments have to be developed.

Cellulose as one of the most abundant natural polymers has been widely used in fiber and film production, and due to its sustainability and excellent mechanical properties, new investigations are devoted to the development of advanced processing technologies and economically feasible applications.[5−7] Recently, a breakthrough technology has been developed to process cellulose (denoted as Ioncell-F) in which ionic liquids (ILs) are used as a green solvent and the dissolved cellulose is then regenerated in water, allowing for an energy-efficient and emission-free production of high-quality fibers.[8] Different from the commercial cellulose fiber process Lyocell, where a high processing temperature and a stabilizer are needed, Ioncell is processed under milder process conditions; thus, cellulose is less degraded, which contributes to both a higher fiber yield and better mechanical strength properties.[8] Besides, the Ioncell technology also enables the incorporation of functionalities directly into the fiber body while maintaining the high mechanical properties and typical soft feel of the Ioncell fiber.[9,10] This opens avenues toward functional textiles.

One target functionality in wearable textile sensors is UV dose detection. Exposure to UV irradiation causes multiple skin damages from the photo-aging of the skin (e.g., wrinkling) to the more severe skin cancer.[11−14] Next to protective measures, a textile-based UV sensor could raise awareness toward the presence and intensity of hazardous UV irradiation.

Received: August 30, 2021
Revised: November 12, 2021
Published: November 23, 2021

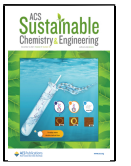

There are generally two mechanisms for UV detection: (1) photoelectric sensors that convert UV irradiation into an electrical output and (2) photochromic sensors in which the material undergoes a series of photochemical reactions giving a direct read-out.[15,16] While photoelectric UV sensors require a complex design to incorporate an external electric field, photochromic sensors offer direct color signals upon UV irradiation without requiring complex or expensive analytical tools.[17−19] Therefore, it is more feasible and economic to incorporate photochromic sensors into a garment to achieve UV-detecting wearable textiles.

Photochromic dyes have been incorporated into synthetic polymer fibers during electrospinning to demonstrate the UV-sensing functionality in textiles.[20−23] A spiropyran-based photochromic dye was doped into a polycaprolactone fiber to detect UV irradiation and the fabricated yarn demonstrated high UV sensitivity.[24] However, photobleaching of the photochromic fibers was observed over time, and the sensitivity dropped 40% after 20 cycles, which is a common limitation for organic photochromic molecules. Besides, the thermal bleaching of organic photochromic compounds limits their applications where high processing temperature is required, for example, dry wet jet spinning of sustainable cellulose fibers. A more durable and chemically more stable photochromic material is demanded to gain UV detection functionality in Ioncell fibers.

A common problem for photochromic materials is low stability toward real-world influences. In contrast, a relatively recent report of inorganic synthetic hackmanite minerals $(Na,M)_8Al_6Si_6O_{24}(Cl,S)_2$ showed excellent reversible UV detection properties. This material develops coloration upon UV irradiation and gets photobleached by artificial or natural white light.[16] By controlling the dopants M, the electronic states of hackmanites can be tailored and the coloration threshold energy can be modified, resulting in good selectivity for UVA, UVB, or UVC radiation. The coloration of hackmanite is based on the quantum energy levels of trapped electrons; therefore, it has better durability than organic photochromic compounds in which the coloration involves drastic changes within the molecular structure. In addition, the size of hackmanite particles can be controlled to be less than 5 μm, which is suitable for the incorporation into textile fibers with a diameter of 10−15 μm.

In this work, we combine the advanced cellulose fiber manufacture technique Ioncell-F process and a non-toxic synthetic hackmanite mineral to achieve sustainable UV detection textiles by direct incorporation of functionalities into the fiber body. Using nanofibrillated cellulose as a dispersant combined with mechanical treatment, the hackmanite particles are homogeneously dispersed in the cellulose dissolution and the resulted hackmanite dope showed excellent spinnability. As a result, we successfully manufactured high-performance UV detection fibers with high mechanical strengths which are comparable with commercial Lyocell cellulose textile fibers. Subsequently, the fibers were knitted into a jersey fabric to demonstrate the feasibility and functionality of the UV detection fabric. Intensive washing and abrasion tests were symmetrically performed to investigate the wash fastness and durability of the hackmanite fabric.

MATERIALS AND METHODS

Pulp. The birch prehydrolyzed kraft dissolving pulp (η = 446 mL/g M_n = 50.3 kDa, M_w = 156.4 kDa, PDI = 3.1) used in this work is received as sheets from Stora Enso (Finland). The sheets were ground using a Wiley mill, and the dry matter content was determined before dissolution in ILs.

Ionic Liquids. 1,5-Diazabicyclo[4.3.0]non-5-ene (DBN, 99%, Fluorochem, UK) was neutralized with an equimolar amount of acetic acid (OAc, glacial, 100%, Merck, Germany). The mixture was kept at 70 °C to avoid the crystallization of the IL during neutralization. The solution mixture was subsequently stirred for another 30 min to ensure complete conversion to [DBNH][OAc].

Hackmanite. The hackmanite material was synthesized with a solid-state reaction route described below. The starting materials were zeolite A (Sigma-Aldrich, reagent grade), NaCl (J. T. Baker, >99.5%), and Na_2SO_4 (Merck, >99%). The samples were prepared by weighing stoichiometric amounts of reagents, that is, 7.00 g of zeolite A (dried at 500 °C for 1 h), 2.40 g of NaCl and 0.60 g of Na_2SO_4. The mixture of these powders was ground by hand in an agate mortar and poured into an alumina crucible. The mixture was then heated at 850 °C (rate 10.0 °C/min) in an air atmosphere for 5 h and let to cool passively to room temperature. After this, the sample was ground in an agate mortar by hand and again heated at 850 °C (rate 10.0 °C/min) in a flowing N2/H2 (88/12%) atmosphere for 2 h and let to cool passively to room temperature. Finally, the sample was ground once again in an agate mortar by hand and finally ground in a Philips Minimill PW4018/00 for 10 min at speed 10 in order to decrease the average particle size to a desirable level.

Cellulose Nanofibrils. Cellulose nanofibrils (CNFs) were prepared as described previously by Österberg et al. (2013).[25] The hardwood kraft pulp was washed into a sodium form and then disintegrated through a high-pressure fluidizer (Microfluidics, M-110Y, Microfluidics Int. Co., Newton, MA) in six passes.

Dispersion of Hackmanite in ILs. Hackmanite particles were added to the 0.4 wt % CNF water suspension to obtain a hackmanite concentration of 5 wt %. The mixture was stirred under ambient conditions overnight and then tip sonicated (Digital Sonifier, Branson) with 30% amplitude for 3 × 30 s. The samples were imaged using an Axio LTS420 (Zeiss) heat-plate microscope to study the dispersion of hackmanite.

Dope Preparation. The hackmanite particles dispersed with CNFs were added to the IL and tip sonicated to further enhance the dispersion, and the mixture was then transferred into a vertical kneader, and cellulose pulp was then added to prepare a 13 wt % cellulose dope. The cellulose pulp was dissolved by kneading at 80 °C at 30 rpm for 2−2.5 h under a vacuum of around 20 mbar. Subsequently, the dope was press-filtered through a layered filter mesh (GKD Ymax2, 5 μm nominal, Gebr. Kufferath AG, Germany) at 80 °C to remove undissolved cellulose fibers. The filtrated dope was stored at 5 °C before spinning.

Oscillation Rheology. Before spinning, the dope was analyzed by oscillation rheology to estimate the spinning temperature. The complex viscosity (η^*) and the dynamic moduli (G′ and G″) of all spinning dopes were analyzed as a function of the shear rate (ω) using an Anton Paar MCR 302 rheometer with a plate and plate geometry (1 mm gap size, 25 mm plate diameter). A strain of 0.5% was selected for the dynamic frequency sweep measurements in a temperature range of 60−80 °C. The zero-shear viscosity, η^0, was determined by fitting the complex viscosity data to the cross-viscosity model.

Fiber Characterization. The mechanical properties of the spun fibers in the conditioned and wet state were determined by using a Favigraph automatic single-fiber tester (Textechno H. Stein GmbH & Co., Germany) based on the ISO 5079 standard (20 mm gauge length, 0.06 cN/tex pretension, 20 mm/min test speed, fiber count 20). All the fibers were conditioned overnight [20 ± 2 °C, 65 ± 2% relative humidity (RH)] before the testing. The slopes of the individual stress−strain curves were used to calculate the elastic modulus of the spun fibers according to ASTM standard D2256/D2256. The fiber's total orientation, f_t, was characterized using a polarized light microscope (Zeiss Axio Scope) equipped with a 5λ Berek compensator. The birefringence, Δn, was calculated by dividing the retardation of the polarized light by the fiber diameter. f_t was then determined by dividing Δn by the maximum birefringence of cellulose

https://doi.org/10.1021/acssuschemeng.1c05938
ACS Sustainable Chem. Eng. 2021, 9, 16338−16346

(0.062).[26] The morphology of hackmanite particles, the surface, and the cross section of spun fibers were imaged using scanning electron microscopy (SEM, Sigma VP Zeiss). All the samples were sputter-coated with gold/palladium (80 Au/20 Pd) for 90 s with a Q 150R S plus (Quorum) sputter to improve the conductivity.

Reflectance Measurements. The fibers were cut into small pieces and arranged in a 1 × 1 cm square. The samples were irradiated with a 254 nm UV light (UVP UVLS-24, 4 W) for 5 min after which the reflectance was measured with an Avantes AvaSpec ULS2048CL-EVO spectrometer coupled with an Avantes FC-IR600-1-ME-HTX optical fiber. The light source was a 60 W incandescent lamp directed toward the sample 50 cm away. The integration time was 160 ms with 10 measurements per sample. The absolute UVC irradiance measurements were conducted with an Opsytec Dr. Gröbel Radiometer RM 12 irradiance meter connected to a UVC probe.

Monofilament Spinning. A small dope (about 20 g) was inserted into a monofilament dry jet wet spinning unit (Fourné Maschinenbau GmbH) and heated up to its spinning temperature (65−75 °C) predicated according to its rheological properties. The diameter of the capillary was 100 μm and the length was 20 μm. The dope was extruded through an air gap (1 cm) into a water coagulation bath where the cellulose was regenerated. The extrusion velocity was kept constant, while the take-up velocity (the speed of the godets collecting the fibers) was changed to collect fibers at different draw ratios (DRs). The collected filaments were cut and washed with 80 °C water for 2 h to remove the residual IL.

Multifilament Spinning. The spinning process is similar to monofilament spinning, but a 400-hole spinneret was used. The amount of dope used for spinning is much bigger, around 1.6 kg.

Fiber Finishing and Opening. The air-dried fibers were immersed in an aqueous finishing solution (Afilan CVS and Leomin PN 80:20) at 50 °C for 5 min to reduce the fiber friction and static properties. The excess water was removed by pressing to reach fourfold of its oven-dry weight and was then air-dried. The targeted amount of spin finish was 0.25% based on the mass of dry fibers. Afterward, the spin-finished fibers were opened with a fiber opener (Trash Analyzer 281C Mesdan Lab, Mesdan S.p.A. Italy).

Yarn Spinning. The spin-finished staple fibers were first conditioned at 65% RH overnight and then carded (Mesdan Lab carding machine 337A) in batches (25 g) to obtain a thin web of fiber fleece, which was formed into a sliver and further elongated and doubled twice with a draw frame (Mesdan Stiro Roving Lab 3371). After drafting, the thinner sliver was doubled, drawn, and false twisted to form a roving. The yarn was spun with a ring spinning machine (Sermates Ring Lab 82 BA). The target count of yarn was 30 tex. The yarn twist direction was Z and twists per meter were 600. The spinning speeds were 10,000−12,000 rpm.

Tensile Testing of Spun Yarn. The tenacity and elongation at break of the spun yarns were determined using an MTS 400 tensile tester equipped with a 50 N load cell using a gauge length of 250 mm and a test speed of 250 mm/min. The yarn was conditioned at 65% RH overnight before the tensile testing.

Fabric Fabrication. Two ring-spun yarns were plied and twisted together (Agteks DirecTwist) to form a 30 tex × 2 S 300 yarn. The plied yarn was knitted into a jersey fabric structure (Stoll CMS ADF 32W E7.3 multi gauge) for fabric testing. Intarsia structure fabrics from both Ioncell and SensoGlow yarns were knitted for showpieces.

Fabric Characterization. The washing test was performed according to EN ISO 105-C06 (AS1 testing procedure). Afterward, the washed fabric was characterized by the reflectance measurement to investigate the SensoGlow particles' fastness. The fabric abrasion resistance was determined by following the Martindale method EN ISO 12947-2:2016. The pilling, fuzzing, and matting of the fabric were tested using the Martindale method according to EN ISO 12945-4:2020.

RESULTS AND DISCUSSION

Fabrication of UV-Sensing Fibers. The main factor governing the mechanical properties of composite materials is the dispersion of the inorganic component in the desired solvent or polymer matrix.[27,28] Especially to achieve good spinnability in dry jet wet spinning, the additives in the cellulose dope must be dispersed homogeneously; otherwise, larger aggregates will lead to the breakage of filaments during spinning. Therefore, the dispersion of hackmanite in [DBNH][OAc] is investigated first.

The hackmanite particles have an average diameter of 1−2 μm but form 25−50 μm aggregates in [DBNH][OAc]. To improve the dispersion quality of hackmanite particles in [DBNH][OAc], we add Trition-100, a commercial nonionic surfactant, and natural CNFs. CNFs have been shown to enhance the dispersion of 2D carbon materials, such as graphene, and inorganic particles, such as $CaCO_3$, as the presence of both −OH group-decorated hydrophilic planes and −CH moieties constitute a hydrophobic plane in its structure.[29−31] The aggregation of hackmanite was significantly decreased by mixing with dispersants (Figure S1). However, mixing with a stirrer cannot generate enough mechanical forces that can break down the aggregates that are already formed. Therefore, to further reduce the size of the aggregates, stronger mechanical forces need to be applied. Both bath sonication and tip sonication were tested to enhance the dispersion. As shown in Figure S2, the mechanical forces generated by bath sonication were not strong enough to break down the hackmanite aggregates, and the particles sedimented after 1.5 h of sonication. Tip sonication, which can generate a stronger force in a confined area, was shown to enhance the dispersion of hackmanite significantly, especially in the presence of CNFs (Figure S3). There is no obvious aggregation of hackmanite observed after tip sonication with CNFs.

The viscoelastic properties, especially the crossover point (COP, at which the G′ and G″ intersect as a result of the transition of a liquid-like state to a solid-like state) and zero shear viscosity, are the two key parameters to evaluate and predict the spinnability of dopes. A spinnable dope should exhibit a zero shear viscosity η^{0}* of 20−40 kPa s and a COP between 2 and 4 kPa at their spinning temperatures.[32] The rheological properties of the cellulose dope incorporated with 0−10% hackmanite and the maximum DR of the fiber spinning are summarized in Table 1 and Figure 1.

Table 1. Rheology Properties and Spinnability of Hackmanite-Incorporated Cellulose Dope at 75 °C

hackmanite wt %	cellulose wt %	η^{0}* Pa·s	COP (G′ = G″) Pa	shear rate rad/s	max. DR
0	13	33,792	3815.1	0.84	14
2	13	30,925	3239.8	0.838	11.7
3.5	13	25,188	3373.2	0.903	10
5	13	28,874	3373.2	0.903	11
10	13	24,257	4094.3	1.09	10.2

A typical shear thinning behavior is observed for all the cellulose dissolutions due to the orientation of cellulose molecules with an increasing angular frequency (Figure 1b), which is critical for the extrusion of cellulose dissolution at the spinneret. It also prevents breakage upon stretching at the air gap where uniaxial stress is applied to reduce the linear density of the filament and increase the orientation of the cellulose chain. However, at a very low angular frequency, a Newtonian plateau is dominant. Thus, the zero shear viscosity η^{0}* can be obtained by applying either the Cross or the Carreau model

https://doi.org/10.1021/acssuschemeng.1c05938
ACS Sustainable Chem. Eng. 2021, 9, 16338−16346

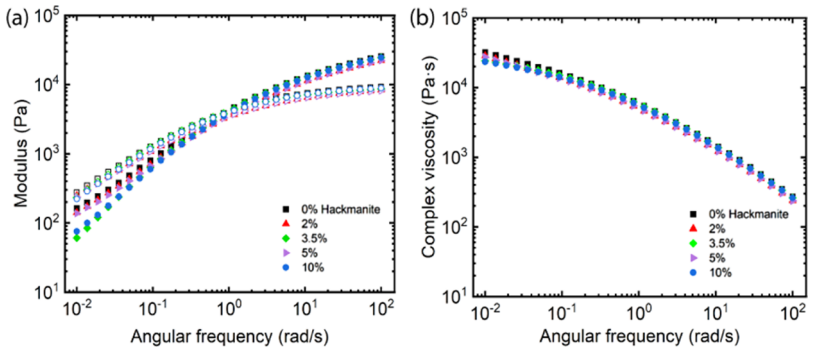

Figure 1. (a) Dynamic moduli and (b) complex viscosities of the hackmanite-incorporated cellulose dissolutions in [DBNH] [OAc] as a function of the shear rate (ω) at 75 °C.

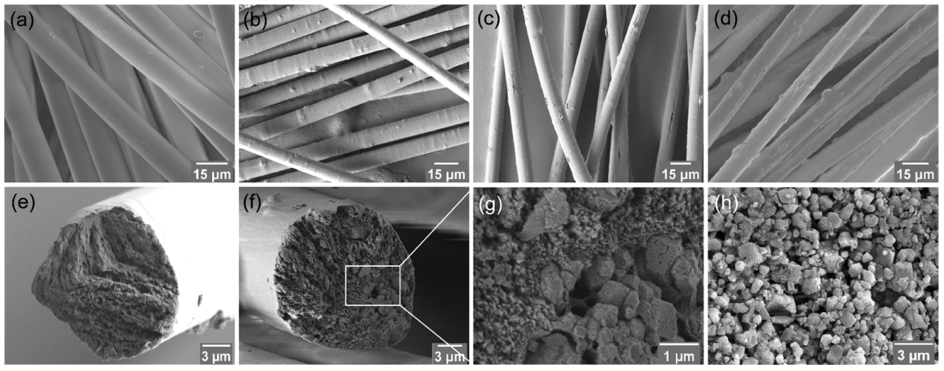

Figure 2. Morphology of the spun fibers and hackmanite particles imaged with SEM. (a) Surface of a standard 13 wt % cellulose fiber. (b) Fiber incorporated with 3.5 wt % hackmanite particles. (c) Fiber incorporated with 5 wt % hackmanite particles. (d) Fiber incorporated with 10 wt % hackmanite particles. (e) Cross section of a standard cellulose fiber. (f) Cross section of a fiber with 3.5 wt % hackmanite particles. (g) Magnification of hackmanite particles incorporated in a cellulose fiber. (h) Hackmanite particles.

presuming that the Cox−Merz rule is valid.[33] The η^0* of hackmanite-incorporated dopes is from 24 to 31 kPa·s with 10−2% hackmanite, respectively, which is slightly lower compared to pure cellulose dope (34 kPa·s), but it is still in the range of a good spinnable dope.

The COP provides valuable information on the molecular mass distribution of the cellulose and the elastic properties of the dope. A monodispersed polymer solution with long molecular chains usually exhibits a high dynamic modulus with a low shear rate at their COP.[34] However, for the hackmanite-incorporated dopes, the molecular mass of cellulose remained the same since there is no special treatment for the cellulose. The shift of the COP to a higher angular frequency derives from the addition of hackmanite particles.

The effect of particles on the rheological properties of polymers is rather complicated; it is influenced by the particle dimensions, their volume fractions, and their interactions with the solvent and polymer molecules in the system.[35−37] Adding rigid particles to a polymer solution typically will increase the dynamic modulus and viscosity, attributed to the hydrodynamic effects of solid particles under flow.[36] Because of the volume fraction of solid particles, the applied straining motion is concentrated in the interstitial polymer solution, which will increase the corresponding stress. However, a drop in the viscosity in a weakly interacting particle-polymer system is also reported, which is explained by a reduced entanglement density of the polymer.[37] The polymers in a confined space have to stretch in the direction parallel to the interface to fit between the rigid particles; thus, the molecules are less entangled.[37] The hackmanite particles have very weak interactions with cellulose, and they are distributed in the entangled cellulose chains; therefore, the addition of hackmanite particles will decrease the η^0* of cellulose dope by disrupting the cellulose network. In our previous studies, the incorporation of gold and silver nanoparticles has tuned the rheology behavior of the cellulose dope in a similar manner.[9]

The hackmanite-incorporated dopes have a good spinnability, which can reach DR 10−12. The spinning behavior of dopes with a cellulose concentration of 13 wt % was categorized as follows based on the measurements in our previous spinning trials: DR < 2, not spinnable; DRs 2−8, poor; DRs 8−12, good; and DR > 14, excellent spinnability. To achieve the required linear density (1.3 dtex) of a commercial textile fiber, the DR needs to reach 11 for a standard Ioncell dope with a cellulose concentration of 13%. From the single filament spinning trials, the cellulose dope with less than 10% hackmanite potentially could be spanned to fibers that meet the requirement for commercial textile fibers. Therefore, multiple filament spinning was tested with a 13% cellulose dope with 3.5% hackmanite, and the results will be discussed in the next section.

Structural and Photo-Responsive Characteristics of UV-Sensing Fibers. The surface of textile fibers, together with the mechanical properties (including fiber strength, elongation, elastic modulus, etc.), is a very important characteristic affecting the quality of fabrics and apparel. As shown in Figure 2a, the standard Ioncell fiber has a very smooth surface, resulting in a splendid silky glow. Although the majority of the hackmanite particles are affirmatively

https://doi.org/10.1021/acssuschemeng.1c05938
ACS Sustainable Chem. Eng. 2021, 9, 16338−16346

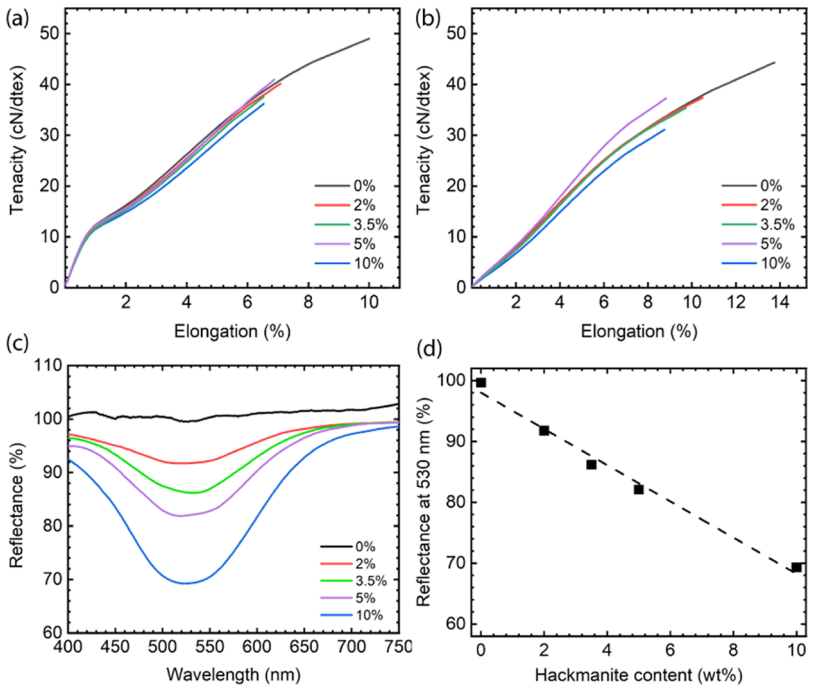

Figure 3. Fiber properties of the hackmanite-incorporated filaments spun with the monofilament spinning unit. The hackmanite content is from 0 to 10%. (a) Stress−strain curves of hackmanite-incorporated fibers measured at 50% RH. (b) Stress−strain curves of hackmanite-incorporated fibers measured in the wet state. (c) Reflectance spectra of the hackmanite-incorporated fibers after UVC irradiation. (d) Reflectance of hackmanite-incorporated fibers at 530 nm. The fibers are irritated with UVC for 5 min before the reflectance spectra measurement.

embedded in the cellulose matrix revealed by the cross-sectional image of the hackmanite fiber (Figure 2f,g), there are a small fraction of hackmanite particles that are close to the surface and create bumps on the fiber surface and thus increase the roughness (Figure 2b−d). When the hackmanite content is below 5%, the surface morphology of the fibers does not change significantly, and fiber surfaces are relatively smooth. With 10% hackmanite content, a higher surface roughness results.

The mechanical properties of the hackmanite-incorporated fibers are generally slightly reduced compared to standard cellulose fibers, meaning that both the maximum tenacity and elongation are decreased even though the stiffness or Young's modulus remains the same. The tenacity of standard cellulose fibers could reach 50 cN/dtex measured at 50% RH, while the fibers incorporated with 2−10% hackmanite have a tenacity of 35−40 cN/dtex. Even though the tenacity dropped by 20−30% when incorporating hackmanite, it is still comparable with commercial Tencel fibers, which is reported to be 36−37 cN/dtex typically.[38] The decrease in the mechanical strength of hackmanite-incorporated fibers is due to weak interfacial adhesion of hackmanite and cellulose, confirmed also by rheology measurements. The mechanical strength of composite materials strongly depends on the stress transfer between the particles and the matrix.[39] For the particles that have strong interfacial adhesion with the matrix, the applied stress can be effectively transferred to the particles from the matrix, and this will clearly improve the mechanical strength.[39] However, for poorly bonded micro-particles, it will reduce the strength of the polymer matrix.[40,41] In addition, some of the hackmanite particles are exposed to the fiber surface instead of embedding inside the fiber (Figure S4). The exposed particles do not have a strong bonding with the cellulose matrix, which will behave like defects during the tensile testing, leading to the breakage of the fibers eventually.

The hackmanite particles are incorporated into cellulose fibers to achieve UV-sensing textiles that show coloration under UV irradiation. To characterize the UV-sensing capability of our hackmanite fibers, we measured the degree of coloration upon UV irradiation as a function of the content of the incorporated particles. Hackmanite fibers with different amounts of particles were irradiated for 5 min with UV irradiation, and then the coloration was measured with reflectance spectroscopy. Figure 3c shows that with increasing particle loading, a higher decrease in reflectance is observed compared to no reflectance change for the unmodified fibers. The decrease in reflectance is a direct result of the absorption of around 530 nm due to the coloration of the material. For the highest particle loading of 10 wt %, a total relative reflectance decrease of 30% is obtained, whereas even a loading of only 2 wt % still gives a detectable reflectance readout. Furthermore, the reflectance decreased at 530 nm scales linearly with the introduced content of particles, underlining the robustness of fabrication as well as the sensitivity range of the hackmanite fibers (Figure 3d).

Fabrication of a UV-Sensing Yarn. The single-filament spinning demonstrated that the hackmanite-incorporated dopes exhibit good spinnability and the produced fibers meet the requirements for both UV detection and mechanical properties. In order to scale up the production of hackmanite fibers toward the fabrication of textiles, we investigated the spinnability of hackmanite-incorporated dopes in multiple filament spinning using a spinneret with 400 capillaries. The best spinnability was achieved with 3.5% hackmanite, and the fibers were collected at DR 11. The mechanical properties and birefringence of hackmanite fibers, standard cellulose fibers, and Tencel fibers are summarized in Table 2. At DR 11, the

https://doi.org/10.1021/acssuschemeng.1c05938
ACS Sustainable Chem. Eng. 2021, 9, 16338−16346

Table 2. Mechanical Properties and Birefringence of a Standard Cellulose Fiber, a 3.5% Hackmanite Fiber, and a Commercial Cellulose Fiber (Tencel)

		conditioned		wet		birefrigence	
sample	titer (dtex)	tenacity (cN/dtex)	Young's modulus (GPa)	tenacity (cN/dtex)	Young's modulus (GPa)	Δn	f_{total}
standard	1.30 ± 0.14	50.5 ± 3.5	21.8 ± 4.5	45.7 ± 4.2	4.3 ± 0.46	0.0455 ± 0.0029	0.733 ± 0.046
3.5% hackmanite	1.31 ± 0.12	37.9 ± 2.7	21.4 ± 2.6	37.2 ± 2.2	4.49 ± 0.57	0.0444 ± 0.0028	0.715 ± 0.045
Tencel	1.27 ± 0.22	36.8 ± 2.7		33.0 ± 3.6			

titer of the hackmanite fiber is around 1.3, which meets the requirement for textile fibers. Even though the tenacity of the hackmanite fiber is reduced compared with the standard cellulose fiber, it is still slightly better than Tencel, which is the current state-of-the-art commercial cellulose textile fiber.

The yarn is manufactured by twisting short staple fibers together to make a single thread. The appearance of the yarn from hackmanite fibers and standard cellulose fibers is quite similar, as shown in Figure 4. The mechanical strength of the yarn is a key parameter for its quality, and resisting slippage depends on the fiber strength and the friction between fibers. The fibers produced by multiple filament spinning are spin finished before yarn spinning to give lubricity and antistatic characteristics to the fibers. From Figure 4b, the breaking tenacity of the spun yarn decreased 30% with the addition of 3.5% hackmanite, and this is mainly derived from the reduced strength of hackmanite fibers. However, hackmanite yarn has a breaking tenacity similar to that of Tencel yarn, indicating a yarn quality suitable for textile applications. Additionally, the statistical distribution of yarn properties is investigated, and interestingly, the mechanical properties of hackmanite yarn are less scattering. The hackmanite fibers have a rougher surface that increases the fiber cohesion and thus improved the yarn spinnability and contributed to less scattering properties.

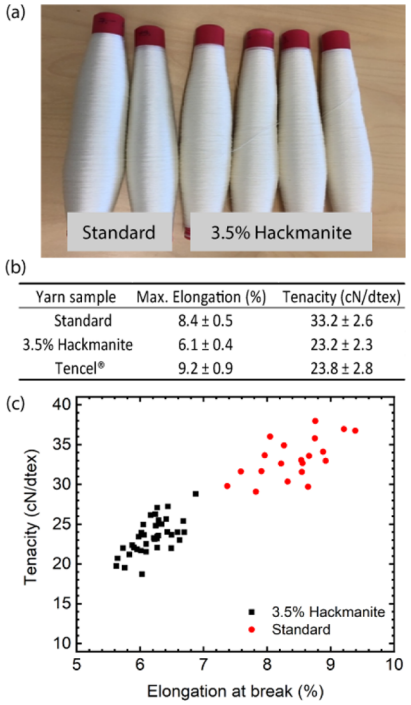

Figure 4. Comparison of the properties of the standard cellulose yarn and 3.5% hackmanite yarn: (a) appearance of the collected yarn; (b) mechanical properties; and (c) statistical distribution of tenacity and elongation.

Fabric Manufacture. The hackmanite yarn was knitted into a jersey fabric structure to demonstrate the potential application of the hackmanite fabric for the detection of UV irradiation. The hackmanite fabric was irradiated from 1 to 5 min under UV light to investigate the correlation of coloration with UV irradiation. The correlation of UV dose values calculated from UVC irradiance * exposure time and color intensity are plotted in Figure 5a. Although the obtained color change under UV irradiation is rather small and difficult to distinguish by naked eyes, it is easily detectable from the red−green−blue ratio. The clear correlation between the color intensity and the UVC dose (Figure 5a) indicated the high potential for utilization in UV dosimetry with cell phone detection. A UV detection textile patch will consist of two parts: the reference pristine cellulose textile that does not change color under UV irradiation and the UV-sensing textile. As illustrated in Figure 5c, an image of the textile patch is captured with a cell phone, and the reference textile is used to calibrate the color intensity. The UV index will then be calculated from the color intensity using RGB values.

The coloration of hackmanite is based on the tenebrescence mechanism; thus, the color intensity is limited by the number of photochromic clusters in the material and also by the coloration ability of the hackmanite material, which varies from batch to batch.[16] The previous study shows that reaching a full tenebrescence color intensity of hackmanite is not an instant process; it requires some time and eventually, there will be a saturation of the color intensity. As shown in Figure 5a, the change of color intensity is detectable at a UV dose of 10 mJ/cm^2 and slowly gets saturated at 5000 mJ/cm^2.

To demonstrate the potential of integrating UV-sensing textiles in everyday wear garments, we investigated the UV-sensing functionality after intensive laundry and abrasion tests. As shown in Figure 5b, the hackmanite fabric maintains its UV-sensing functionality for over 18,000 abrasion cycles, 2000 pilling cycles, and laundry with detergent, which meets the standard textile benchmarks, demonstrating its potential for industrial production.

CONCLUSIONS

In summary, we demonstrated the feasibility of incorporating a photochromic mineral hackmanite directly into the cellulose matrix during the dissolution in ILs to achieve UV detection fibers using dry jet wet spinning. The challenge of dispersing hackmanite particles in an IL is tackled by tip sonication in the presence of CNFs as a dispersant, resulting in homogeneously distributed particles among the fiber cross sections, further contributing to a good spinnability. Up to 10% of particles can be incorporated into the cellulose dope while maintaining good spinnability. The mechanical strength of the UV detection fibers is comparable with the commercial regen-

https://doi.org/10.1021/acssuschemeng.1c05938
ACS Sustainable Chem. Eng. 2021, 9, 16338−16346

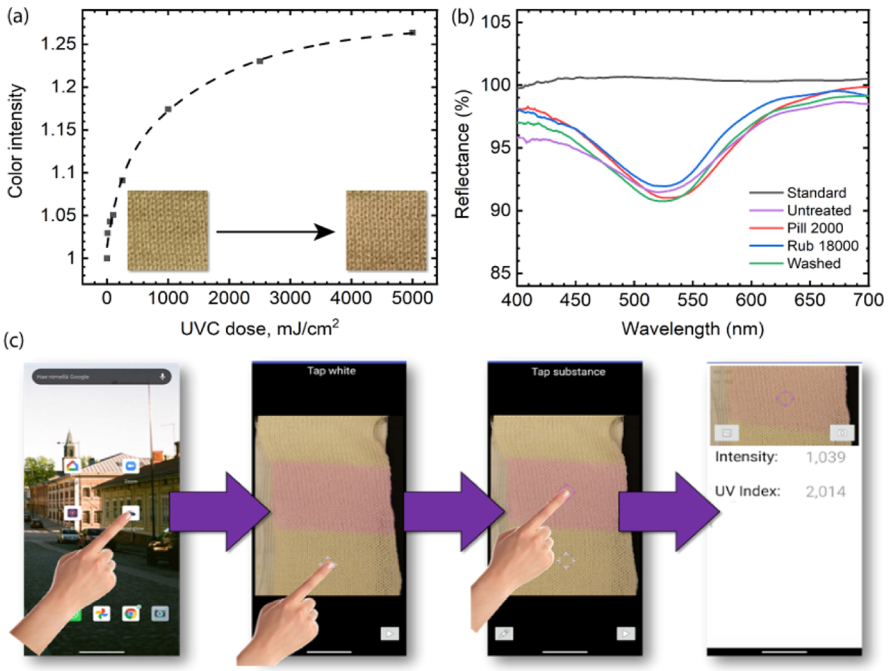

Figure 5. Functional characterization of a fabric knitted from 3.5% hackmanite staple fibers. (a) UVC dose detected with the hackmanite fabric. The color intensity was analyzed using the ImageJ program. The insets show the color change of the fabric from 0 to 5000 mJ/cm^2 UV doses. (b) Reflectance spectra of the hackmanite fabric after pilling, abrasion, and laundering tests (number indicates cycles in the Martindale device). The standard fabric is knitted from pure cellulose fibers. (c) Illustration of UV index measurements using a cell phone using an ad hoc mobile application made specifically for measuring changes in a material with hackmanite.[42]

erated cellulose fibers with a breaking tenacity of 35−40 cN/dtex.

The photochromic mineral-doped cellulose fibers showed high sensitivity and fast response to UV irradiation, and a linear relationship between the hackmanite content and coloration was revealed. As a proof of concept, a piece of jersey fabric is knitted to demonstrate its use in wearable UV sensors. The color changes of the fabric induced by UV irradiation can be easily analyzed by a cell phone app and then correlated to a UV index. Since the color change is not so visible by the naked eyes but rather sensitive to the RGB ratio analysis instead, it provides an opportunity to achieve UV-sensing functionality and maintains the aesthetic appearance of the garment. Furthermore, the UV-sensing fabric exhibited excellent wash fastness and resistance to abrasion, confirming its potential to be integrated into daily wear and the possibility of reducing the release of photochromic particles into the environment, providing a more sustainable way to fabricate functional textiles. With an adequate adaptation of the process, it may enable recycling the photochromic textiles using Ioncell technology to achieve a circular economy of textiles.

■ ASSOCIATED CONTENT

Supporting Information

The Supporting Information is available free of charge at https://pubs.acs.org/doi/10.1021/acssuschemeng.1c05938.

Optical microscopy images of hackmanite particles dispersed in [DBNH][OAc] and SEM images of hackmanite particles incorporated in cellulose fibers (PDF)

■ AUTHOR INFORMATION

Corresponding Authors

Wenwen Fang − *Department of Bioproducts and Biosystems, Aalto Univerisity, FI-02150 Espoo, Finland;* orcid.org/0000-0003-2645-9752; Email: wenwen.fang@aalto.fi

Herbert Sixta − *Department of Bioproducts and Biosystems, Aalto Univerisity, FI-02150 Espoo, Finland;* orcid.org/0000-0002-9884-6885; Email: herbert.sixta@aalto.fi

Authors

Emma Sairanen − *Department of Bioproducts and Biosystems, Aalto Univerisity, FI-02150 Espoo, Finland*

Sami Vuori − *Department of Chemistry, University of Turku, FI-20014 Turku, Finland*

Marja Rissanen − *Department of Bioproducts and Biosystems, Aalto Univerisity, FI-02150 Espoo, Finland*

Isabella Norrbo − *Department of Chemistry, University of Turku, FI-20014 Turku, Finland*

Mika Lastusaari − *Department of Chemistry, University of Turku, FI-20014 Turku, Finland;* orcid.org/0000-0003-1872-0391

Complete contact information is available at: https://pubs.acs.org/10.1021/acssuschemeng.1c05938

Notes

The authors declare no competing financial interest.

■ ACKNOWLEDGMENTS

This project is funded by the Academy of Finland Project WTF-Click-Nano. We would like to thank Simone Haslinger (Reima Oy) for providing knowledge of the textile market and fruitful discussions, Kaniz Moriam (Aalto University) for her support in fiber spinning, and Sami Rantasalo for technical

support in the lab. We acknowledge the provision of facilities and technical support by Aalto University at the OtaNano—Nanomicroscopy Center (Aalto-NMC).

REFERENCES

(1) Islam, G. M. N.; Ali, A.; Collie, S. Textile Sensors for Wearable Applications: A Comprehensive Review. *Cellulose* **2020**, *27*, 6103—6131.
(2) Heikenfeld, J.; Jajack, A.; Rogers, J.; Gutruf, P.; Tian, L.; Pan, T.; Li, R.; Khine, M.; Kim, J.; Wang, J.; Kim, J. Wearable Sensors: Modalities, Challenges, and Prospects. *Lab Chip* **2018**, *18*, 217—248.
(3) Ahmad Tarar, A.; Mohammad, U.; K Srivastava, S. Wearable Skin Sensors and Their Challenges: A Review of Transdermal, Optical, and Mechanical Sensors. *Biosensors* **2020**, *10*, 56.
(4) Gonçalves, C.; Ferreira da Silva, A.; Gomes, J.; Simoes, R. Wearable E-Textile Technologies: A Review on Sensors, Actuators and Control Elements. *Inventions* **2018**, *3*, 14.
(5) Isik, M.; Sardon, H.; Mecerreyes, D. Ionic Liquids and Cellulose: Dissolution, Chemical Modification and Preparation of New Cellulosic Materials. *Int. J. Mol. Sci.* **2014**, *15*, 11922—11940.
(6) Eichhorn, S. J.; Dufresne, A.; Aranguren, M.; Marcovich, N. E.; Capadona, J. R.; Rowan, S. J.; Weder, C.; Thielemans, W.; Roman, M.; Renneckar, S.; Gindl, W.; Veigel, S.; Keckes, J.; Yano, H.; Abe, K.; Nogi, M.; Nakagaito, A. N.; Mangalam, A.; Simonsen, J.; Benight, A. S.; Bismarck, A.; Berglund, L. A.; Peijs, T. Review: Current International Research into Cellulose Nanofibres and Nanocomposites. *J. Mater. Sci.* **2010**, *45*, 1—33.
(7) Moon, R. J.; Martini, A.; Nairn, J.; Simonsen, J.; Youngblood, J. Cellulose Nanomaterials Review: Structure, Properties and Nanocomposites. *Chem. Soc. Rev.* **2011**, *40*, 3941—3994.
(8) Sixta, H.; Michud, A.; Hauru, L.; Asaadi, S.; Ma, Y.; King, A. W. T.; Kilpeläinen, I.; Hummel, M. Ioncell-F: A High-Strength Regenerated Cellulose Fibre. *Nord. Pulp Pap. Res. J.* **2015**, *30*, 43—57.
(9) Haslinger, S.; Ye, Y.; Rissanen, M.; Hummel, M.; Sixta, H. Cellulose Fibers for High-Performance Textiles Functionalized with Incorporated Gold and Silver Nanoparticles. *ACS Sustainable Chem. Eng.* **2020**, *8*, 649—658.
(10) Moriam, K.; Rissanen, M.; Sawada, D.; Altgen, M.; Johansson, L.-S.; Evtyugin, D. V.; Guizani, C.; Hummel, M.; Sixta, H. Hydrophobization of the Man-Made Cellulosic Fibers by Incorporating Plant-Derived Hydrophobic Compounds. *ACS Sustainable Chem. Eng.* **2021**, *9*, 4915—4925.
(11) Amaro-Ortiz, A.; Yan, B.; D'Orazio, J. Ultraviolet Radiation, Aging and the Skin: Prevention of Damage by Topical CAMP Manipulation. *Molecules* **2014**, *19*, 6202—6219.
(12) Biniek, K.; Levi, K.; Dauskardt, R. H. Solar UV Radiation Reduces the Barrier Function of Human Skin. *Proc. Natl. Acad. Sci. U.S.A.* **2012**, *109*, 17111—17116.
(13) Matsumura, Y.; Ananthaswamy, H. N. Toxic Effects of Ultraviolet Radiation on the Skin. *Toxicol. Appl. Pharmacol.* **2004**, *195*, 298—308.
(14) Brash, D. E.; Rudolph, J. A.; Simon, J. A.; Lin, A.; Mckenna, G. J.; Baden, H. P.; Halperin, A. J.; Ponten, J. A Role for Sunlight in Skin Cancer: UV-Induced P53 Mutations in Squamous Cell Carcinoma. *Proc. Natl. Acad. Sci. U.S.A.* **1991**, *88*, 10124—10128.
(15) Zou, W.; Sastry, M.; Gooding, J. J.; Ramanathan, R.; Bansal, V. Recent Advances and a Roadmap to Wearable UV Sensor Technologies. *Adv. Mater. Technol.* **2020**, *5*, 1901036.
(16) Norrbo, I.; Curutchet, A.; Kuusisto, A.; Mäkelä, J.; Laukkanen, P.; Paturi, P.; Laihinen, T.; Sinkkonen, J.; Wetterskog, E.; Mamedov, F.; Le Bahers, T.; Lastusaari, M. Solar UV Index and UV Dose Determination with Photochromic Hackmanites: From the Assessment of the Fundamental Properties to the Device. *Mater. Horiz.* **2018**, *5*, 569—576.
(17) Kim, S. J.; Han, J.-W.; Kim, B.; Meyyappan, M. Single Walled Carbon Nanotube Based Air Pocket Encapsulated Ultraviolet Sensor. *ACS Sens.* **2017**, *2*, 1679—1683.
(18) Zou, W.; González, A.; Jampaiah, D.; Ramanathan, R.; Taha, M.; Walia, S.; Sriram, S.; Bhaskaran, M.; Dominguez-Vera, J. M.; Bansal, V. Skin Color-Specific and Spectrally-Selective Naked-Eye Dosimetry of UVA, B and C Radiations. *Nat. Commun.* **2018**, *9*, 1—10.
(19) Kim, S. J.; Moon, D.-I.; Seol, M.-L.; Kim, B.; Han, J.-W.; Meyyappan, M. Wearable UV Sensor Based on Carbon Nanotube-Coated Cotton Thread. *ACS Appl. Mater. Interfaces* **2018**, *10*, 40198—40202.
(20) Lee, E.-M.; Gwon, S.-Y.; Ji, B.-C.; Wang, S.; Kim, S.-H. Photoswitching Electrospun Nanofiber Based on a Spironaphthoxazine- Isophorone-Based Fluorescent Dye System. *Dyes Pigm.* **2012**, *92*, 542—547.
(21) Wang, M.; Vail, S. A.; Keirstead, A. E.; Marquez, M.; Gust, D.; Garcia, A. A. Preparation of Photochromic Poly(Vinylidene Fluoride-Co-Hexafluoropropylene) Fibers by Electrospinning. *Polymer* **2009**, *50*, 3974—3980.
(22) Khatri, Z.; Ali, S.; Khatri, I.; Mayakrishnan, G.; Kim, S. H.; Kim, I.-S. UV-Responsive Polyvinyl Alcohol Nanofibers Prepared by Electrospinning. *Appl. Surf. Sci.* **2015**, *342*, 64—68.
(23) Zhang, W.-J.; Hong, C.-Y.; Pan, C.-Y. Fabrication of Electrospinning Fibers from Spiropyran-Based Polymeric Nanowires and Their Photochromic Properties. *Macromol. Chem. Phys.* **2013**, *214*, 2445—2453.
(24) Zheng, Y.; Panatdasirisuk, W.; Liu, J.; Tong, A.; Xiang, Y.; Yang, S. Patterned, Wearable UV Indicators from Electrospun Photochromic Fibers and Yarns. *Adv. Mater. Technol.* **2020**, *5*, 2000564.
(25) Österberg, M.; Vartiainen, J.; Lucenius, J.; Hippi, U.; Seppälä, J.; Serimaa, R.; Laine, J. A Fast Method to Produce Strong NFC Films as a Platform for Barrier and Functional Materials. *ACS Appl. Mater. Interfaces* **2013**, *5*, 4640—4647.
(26) Lenz, J.; Schurz, J.; Wrentschur, E. On the Elongation Mechanism of Regenerated Cellulose Fibers. *Holzforschung* **1994**, *48*, 72—76.
(27) Bittmann, B.; Haupert, F.; Schlarb, A. K. Ultrasonic Dispersion of Inorganic Nanoparticles in Epoxy Resin. *Ultrason. Sonochem.* **2009**, *16*, 622—628.
(28) Wieneke, J. U.; Kommoß, B.; Gaer, O.; Prykhodko, I.; Ulbricht, M. Systematic Investigation of Dispersions of Unmodified Inorganic Nanoparticles in Organic Solvents with Focus on the Hansen Solubility Parameters. *Ind. Eng. Chem. Res.* **2012**, *51*, 327—334.
(29) Xiong, R.; Kim, H. S.; Zhang, L.; Korolovych, V. F.; Zhang, S.; Yingling, Y. G.; Tsukruk, V. V. Wrapping Nanocellulose Nets around Graphene Oxide Sheets. *Angew. Chem.* **2018**, *130*, 8644—8649.
(30) Li, Y.; Zhu, H.; Shen, F.; Wan, J.; Lacey, S.; Fang, Z.; Dai, H.; Hu, L. Nanocellulose as Green Dispersant for Two-Dimensional Energy Materials. *Nano Energy* **2015**, *13*, 346—354.
(31) Tenhunen, T.-M.; Pöhler, T.; Kokko, A.; Orelma, H.; Gane, P.; Schenker, M.; Tammelin, T. Enhancing the Stability of Aqueous Dispersions and Foams Comprising Cellulose Nanofibrils (CNF) with CaCo3 Particles. *Nanomaterials* **2018**, *8*, 651.
(32) Michud, A.; Hummel, M.; Sixta, H. Influence of Molar Mass Distribution on the Final Properties of Fibers Regenerated from Cellulose Dissolved in Ionic Liquid by Dry-Jet Wet Spinning. *Polymer* **2015**, *75*, 1—9.
(33) Chen, X.; Zhang, Y.; Wang, H.; Wang, S.-W.; Liang, S.; Colby, R. H. Solution Rheology of Cellulose in 1-Butyl-3-Methyl Imidazolium Chloride. *J. Rheol.* **2011**, *55*, 485—494.
(34) Mezger, T. G. *The Rheology Handbook. European Coatings Tech Files*, 3rd Revised ed.; Vincentz Network, 2011; Vol. *28*.
(35) Jain, S.; Goossens, J. G. P.; Peters, G. W. M.; Van Duin, M.; Lemstra, P. J. Strong Decrease in Viscosity of Nanoparticle-Filled Polymer Melts through Selective Adsorption. *Soft Matter* **2008**, *4*, 1848—1854.
(36) Le Meins, J.-F.; Moldenaers, P.; Mewis, J. Suspensions in Polymer Melts. 1. Effect of Particle Size on the Shear Flow Behavior. *Ind. Eng. Chem. Res.* **2002**, *41*, 6297—6304.

https://doi.org/10.1021/acssuschemeng.1c05938
ACS Sustainable Chem. Eng. 2021, 9, 16338—16346

(37) Tuteja, A.; Mackay, M. E.; Hawker, C. J.; Van Horn, B. Effect of Ideal, Organic Nanoparticles on the Flow Properties of Linear Polymers: Non-Einstein-like Behavior. *Macromolecules* **2005**, *38*, 8000−8011.
(38) Mather, R.; Wardman, R. Regenerated Fibers. In *Chemistry of Textile Fibres*; Royal Society of Chemistry, 2015; pp 111−143.
(39) Pukanszky, B.; Vörös, G. Mechanism of Interfacial Interactions in Particulate Filled Composites. *Compos. Interfaces* **1993**, *1*, 411−427.
(40) Fu, S.-Y.; Feng, X.-Q.; Lauke, B.; Mai, Y.-W. Effects of Particle Size, Particle/Matrix Interface Adhesion and Particle Loading on Mechanical Properties of Particulate-Polymer Composites. *Composites, Part B* **2008**, *39*, 933−961.
(41) Dekkers, M. E. J.; Heikens, D. The effect of interfacial adhesion on the tensile behavior of polystyrene-glass-bead composites. *J. Appl. Polym. Sci.* **1983**, *28*, 3809−3815.
(42) Laine, T.; Norrbo, I.; Holvitie, J.; Lastusaari, M. An Android Application for Determining UV Index and UV Dose from Hackmanite. *Priv Software*, 2020.

https://doi.org/10.1021/acssuschemeng.1c05938
ACS Sustainable Chem. Eng. 2021, 9, 16338−16346